SAND2021-7310C

Towards an Islanding Detection Method Using a Digital Twin Concept

Nelson E. Saavedra-Peña[1], Rachid Darbali-Zamora[2], Edgardo Desarden-Carrero[1], and Erick Aponte-Bezares[1]

[1]University of Puerto Rico-Mayagüez, Mayagüez, Puerto Rico 00682, USA
[2]Sandia National Laboratories, Albuquerque, New Mexico, 87185, USA

***Abstract* —In this paper, the development of a mathematical model for islanding detection method based on the concept of a digital twin is presented. This model estimates the grid impedance seen by a distributed energy resource. The proposed algorithm has characteristics of passive and active islanding detection methods. Using a discrete state-space representation of a *dq0* axis power system as equality constraints, a digital twin is optimized to match the power system of interest. The fundamental concept is to use the estimated grid impedance as the parameter that will identify the difference between normal operation and islanding scenarios. Selecting arbitrary initial values, the proposed method was able to approximate the response of the system and therefore a value for the system impedance. Results indicate that the proposed method has the potential to estimate the grid impedance at the point of common coupling. Further, ongoing work is required to explore possible limitations and challenging scenarios for accurate impedance estimation and eventual islanding detection.**

***Index Terms*—IEEE Std 1547, islanding detection, distributed generation, renewable energy, Lagrange, optimization**

I. Introduction

Power systems are expected to be reliable and resilient when operating under a variety of conditions [1], [2]. Distributed energy resources (DERs) can contribute to the diversity in generation of a power system [3]. When these DERs are subjected to abrupt conditions such as frequency and voltage deviations, unintentional islanding may occur. This means that DERs could disconnect from the grid but remain energized, creating a safety concern for utilities [4], [5]. The IEEE Std 1547-2018 describes the types of islanding that can occur in an electric power system. The two types of islanding are intentional and unintentional islanding [6]. For unintentional islanding, these guidelines not only require DERs connected to a power system to detect when islanded and disconnect, but mandate that these DERs identify the island and trip within two seconds of detection. Moreover, standards require that DERs comply with grid support functionality as well as ride-through capabilities [7]. For this reason, extensive research has been performed in determining effective methods that will successfully identify islanding conditions [8], [9].

A no-detection zone (NDZ) is an area of operation in where the islanding detection methods fails to detect islanding conditions. The NDZ can define the effectiveness of an islanding detection method. An ideal method would have NDZ of zero, or close to zero. Unintentional anti-islanding (UIA) active detection methods may have little NDZ when generation and load are matched. Although active techniques are used frequently, they usually involve positive feedback or injection of disturbances into the system to identify an island [10]. Active techniques may not affect performance when the DER is connected to the power system but will destabilize the DER system when islanded. Alternatively, passive techniques are simple to implement but can have a large NDZ when generation and load are matched. Low distortion of the signal and fast detection time are two main characteristics when using passive techniques. Although both kinds of islanding methods can be combined into hybrid methods, there isn't a single method that would fit every application. On the other hand, due to the ability to detect an islanding condition without trying to destabilize the system, the proposed method can be considered as a passive islanding detection method [11].

Herein, this paper proposes an islanding detection method that uses a discrete state-space representation of a *dq0* axis power system as equality constraints. The fundamental concept is to use the estimated grid impedance as the parameter that will identify the difference between normal operation and islanding scenarios.

II. Proposed Islanding Detection Method

A. Method Description

An effective and non-invasive approach for detecting unintentional islanding is proposed. An overview of the approach is presented in Fig. 1 [11]. A discrete mathematical model represents the real system. The starting point for the model is taken from the initial value of the impedance of the grid. An algorithm then optimizes the value of impedance of the digital twin such that an optimal match is reached. A digital twin is a simulated representation of an actual physical system [12]. This optimal point is reached when the function generated by the digital twin is closest to the measurements of the real system. The equivalent grid impedance in an islanding scenario will tend to be significantly larger than normal operation impedance.

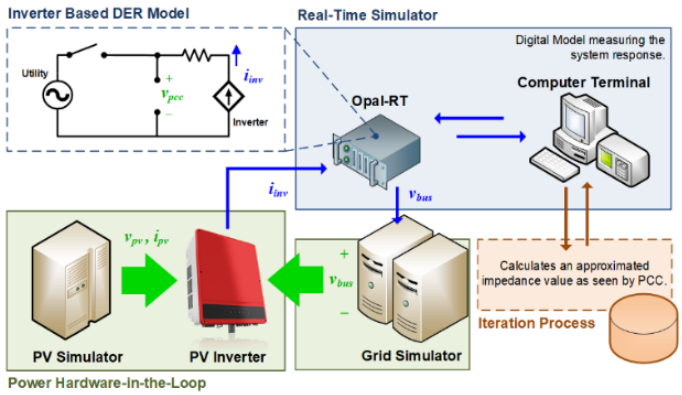

Fig. 1. Digital Model Schematic for Islanding Detection.

B. *Fundamentals of the Concept*

In order to demonstrate the fundamental concepts of the proposed islanding detection approach, an example of a circuit diagram with constant supply voltage and RL load is presented in Fig. 2. The simplified circuit can be analyzed using a simple circuit analysis approach.

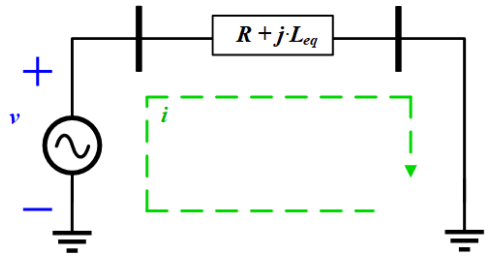

Fig. 2. Example of Circuit Diagram Representing the RL Load.

In this diagram, the resistance of the circuit is represented by the variable R, while L_{eq} represents the equivalent circuit inductance. The voltage equation of the circuit is expressed in equation (1). Where i is the current response of the system and is defined by equation (2). In this equation, $i(0) = 0$, *and* $i(\infty) = V/R$.

$$V = R \cdot i(t) + L_{eq} \cdot \frac{di(t)}{dt} \#(1)$$

$$i(t) = \frac{V}{R} \cdot \left(1 - e^{\left(\frac{-R}{L_{eq}} \cdot t\right)}\right) \#(2)$$

The actual device current and iterations of the estimated value of the digital twin are shown in Fig. 3. The actual current, represents the target current for the optimization algorithm to emulate after iterating the inductance values in order to minimize the error between the actual current and its estimated value. The algorithm is able to yield the estimated system impedance that minimizes the error between the actual system current and the current estimated with the digital twin providing a simulated representation of the actual system. The estimated impedance would become the basis for an islanding detection method.

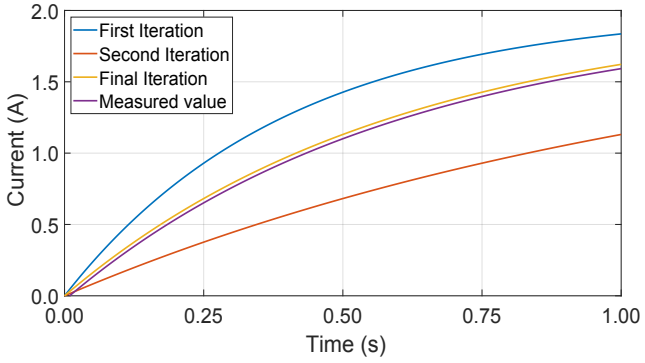

Fig. 3. Example of the Iterative Approximation for the Islanding Detections Approach.

C. *Problem Statement and Modeling*

Using equations (3) through (5) the ordinary differentials equations can be solved for a state vector $x(t)$ given an initial state $x(t_0) = x_0$ and specific input signal $u(t)$. The instant output of a state given a specific input is represented by equation (4). Where A, B, C, and D are represented by matrices of dimension $n \times n$, $n \times p$, $q \times n$, and $q \times p$, respectively.

$$\dot{x} = A \cdot x(t) + B \cdot U(t) \#(3)$$

$$y = C \cdot x(t) + D \cdot U(t) \#(4)$$

$$\dot{x} = f(x,U) \#(5)$$

D. *Cost Function and Optimization*

A discrete representation of the state-space system of equation (3) is shown in equation (6).

$$\dot{x} = A_d \cdot x + B_d \cdot U \#(6)$$

The input matrix U is defined by equation (7).

$$U = [U_1\ U_2\ U_3\ U_4]^T = [V_Q\ V_{QS}\ V_D\ V_{DS}]^T \#(7)$$

V_Q and V_{QS} are the voltage of inverter and equivalent grid voltage referred to the quadrature axis, respectively. V_D and V_{DS} are the voltage of the inverter and equivalent grid voltage in the direct axis, respectively. The discrete state-space model can be derived using equation (8) and equation (9).

$$A_d = e^{A \cdot t} \#(8)$$

$$B_d = inv(A) \cdot (A_d - I) \cdot B \#(9)$$

Introducing the estimated parameter, $\mu = [Z_{TH}]$ into the discrete state-space model in equation (10) yields equation (11), where the variable k represents the number of the iteration.

$$x[k+1] = A_d \cdot x[k] + B_d \cdot U[k] \#(10)$$

$$x[k+1] = A_d(\mu) \cdot x[k] + B_d(\mu) \cdot U[k] \#(11)$$

The equality constraint must satisfy equation (12).

$$H = \dot{x} - f(x,\mu) = 0 \#(12)$$

The discrete representation of equation (12) is shown in equation (13).

$$H_k = x[k+1] - A_d(\mu) \cdot x[k] - B_d(\mu) \cdot U[k] \#(13)$$

The cost function in equation (14) is a quadratic function that represents the error between the state variables of the system and the digital twin. The variable Q is the weight assigned to each state variable of the system, x are the state variables of the system, and the variable x^* is the real-time measured variables. Lagrange's method establishes the conditions for minimizing equation (14), subject to $H_k = 0$. Lagrange's equation is

expressed in equation (15). Finally, the derivative of the Lagrange equation with respect to each of the independent variables is calculated. The derivatives with respect to the independent variables are then said to be equal to zero [14], [15].

$$C(x) = (x - x^*)^T \cdot Q \cdot (x - x^*) \quad \#(14)$$

$$L(x,\mu) = C(x) + \lambda^T \cdot H(x,\mu) \#(15)$$

$$\frac{dL}{dx} = \frac{dC}{dx} + \lambda^T \cdot \frac{dH}{dx} = 0 \#(16)$$

Modifying equation (16), it is possible to obtain the value of the Lagrange multiplier λ using equation (17).

$$\lambda^T = -\left[\frac{dC}{dx}\right] \cdot \left[\frac{dH}{dx}\right]^{-1} \quad \#(17)$$

To calculate dC/dx and dH/dx, equation (18) and equation (19) are used, respectively.

$$\frac{dC}{dx} = 2 \cdot (x - x^*)^T \cdot Q \quad \#(18)$$

$$\frac{dH}{dx} = \begin{bmatrix} \frac{dH_1}{dx[k]} & \frac{dH_1}{dx[k+1]} & 0 & 0 \\ 0 & \frac{dH_2}{dx[k]} & \frac{dH_2}{dx[k+1]} & 0 \\ 0 & 0 & \frac{dH_3}{dx[k]} & \frac{dH_3}{dx[k+1]} \\ 0 & 0 & 0 & \frac{dH_4}{dx[k]} \end{bmatrix} \#(19)$$

The coefficients of the matrix shown in equation (19) are defined by equation (20) and equation (21).

$$\frac{dH}{dx[k]} = -A_d(\mu) \#(20)$$

$$\frac{dH}{dx[k+1]} = I \#(21)$$

Partial derivative, $dL/d\lambda$, must be equal to the equality constraint in equation (22). Then, partial derivative $dL/d\mu$ is calculated as shown in equation (23). The optimization will run until partial derivative $dL/d\mu$ is equal to zero.

$$\frac{dL}{d\lambda} = H(x,\mu) = 0 \quad \#(22)$$

$$\frac{dL}{d\mu} = \lambda^T \cdot \frac{dH}{d\mu} \quad \#(23)$$

In equation (23), variable $dH/d\mu$ is defined by equation (24).

$$\frac{dH}{d\mu} = -x[k] \cdot \left[\frac{dA_d(\mu)}{d\mu}\right] - U[k] \cdot \left[\frac{dB_d(\mu)}{d\mu}\right] \#(24)$$

The variable μ^{k+1} is calculated for the estimated parameter, Z_{TH}, using equation (25).

$$\mu^{(k+1)} = \mu^{(k)} + \alpha \cdot \frac{dL}{d\mu} \#(25)$$

In this equation, variable α is the step size, and $dL/d\mu$ represents the direction. Variable α, can be obtained by iteration dependent on the value of the cost function [16].

III. Modeling at the Point of Common Coupling

The state-space model of the system is shown in Fig. 4. The grid is reduced using power flow analysis [17]. The bus considered as the point of common coupling (PCC) is where the inverter is connected to the grid. Both the grid and the inverter are modeled using an equivalent voltage in series with an impedance. A *dq0* transform is applied to the equivalent circuit to simplify the analysis. Using the two-axis reference frame theory, equivalent circuits in '*q*' and '*d*' axis are shown in Fig. 5, respectively [18]. The state-space model is derived using circuit analysis. Parameter μ must be included as an independent variable in the state-space modeling. Substituting Z_{TH} in equation (23) and equation (24) by μ, the state-space model is then described as dependent on the value of μ. $A(\mu)$ and $B(\mu)$ are then discretized for the optimization algorithm.

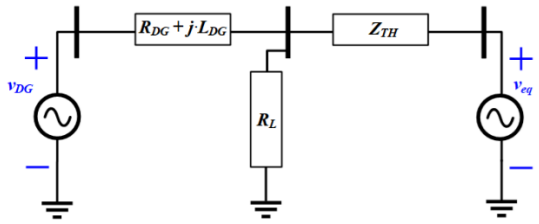

Fig. 4. System One Line Diagram for Equivalent Circuit at PCC.

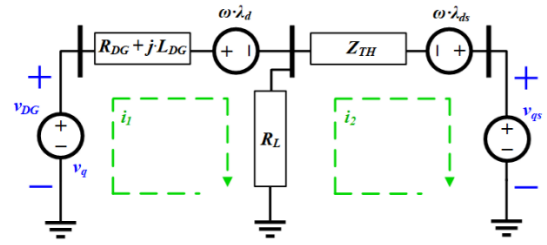

(a)

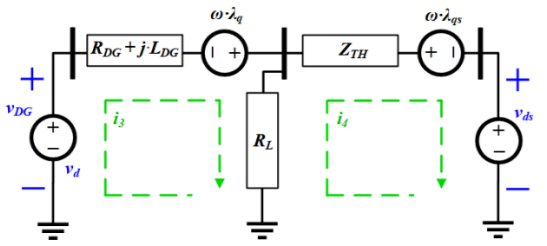

(b)

Fig. 5. Equivalent Circuit Schematic (a) Quadrature Axis Equivalent

Circuit at PCC. (b) Direct Axis Equivalent Circuit at PCC.

$$A = \begin{bmatrix} -\frac{(R_{DG}+R_L)}{L_{DG}} & -\frac{R_L}{L_{DG}} & -\omega & 0 \\ -\frac{R_L}{Z_{TH}} & -\frac{R_L}{Z_{TH}} & 0 & -\omega \\ \omega & 0 & -\frac{(R_{DG}+R_L)}{L_{DG}} & -\frac{R_L}{L_{DG}} \\ 0 & \omega & -\frac{R_L}{Z_{TH}} & -\frac{R_L}{Z_{TH}} \end{bmatrix} \#(23)$$

$$B = \begin{bmatrix} \frac{1}{L_{DG}} & 0 & 0 & 0 \\ 0 & \frac{1}{Z_{TH}} & 0 & 0 \\ 0 & 0 & \frac{1}{L_{DG}} & 0 \\ 0 & 0 & 0 & \frac{1}{Z_{TH}} \end{bmatrix} \#(24)$$

IV. Distribution System Under Test

A case study is described using the power system illustrated in Fig. 6. Using per unit impedance values, shown in Table I, the bus admittance matrix is calculated to reduce the power system into a single impedance in series with an equivalent voltage from the grid.

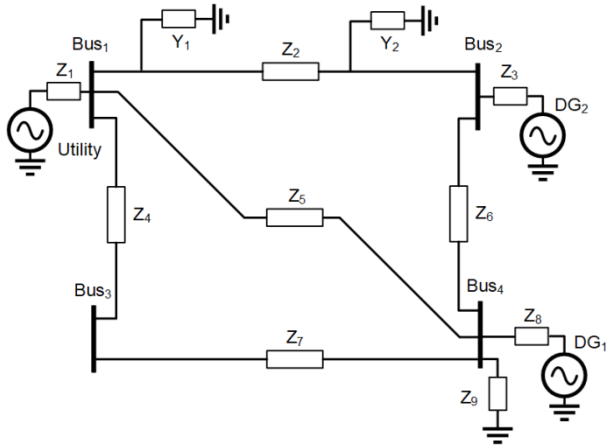

Fig. 6. Power System Diagram of the Case Study.

Table I:
Line Impedance Values in per Unit

Element	*From*	*To*	*Distance (km)*	*Impedance (p.u.)*
Z_1	1	1	5	0.005*i*
Z_2	1	2	3	0.015*i*
Z_3	2	2	1	0.200*i*
Z_4	1	3	6	0.015*i*
Z_5	1	4	10	0.020*i*
Z_6	2	4	2	0.025*i*
Z_7	3	4	4	0.030*i*
Z_8	4	4	-	1 + 0.200*i*
Z_9	4	4	-	1.5
Y_1	1	1	-	0.05125*i*
Y_2	2	2	-	0.05125*i*

V. Simulation Results from MATLAB

An impedance smaller than the real impedance value is selected as the initial impedance. The algorithm finds an impedance similar to the impedance of the grid after 3 iterations, as shown in Table II. The per unit initial value for Z_{TH} is selected to be 0.0130i in this case. The calculated (real) value is Z_{TH} = 0.0146i. For the second part of the case study, the initial impedance, Z_{TH} = 0.0170i, is selected to be larger than the real impedance of the system. The algorithm approximated a value after 6 iterations, as shown in Table III.

Table II:
Iterations for Smaller Initial Impedance

Iteration (k)	Z_{TH} *(p.u.)*
1	0.0130 *i*
2	0.0136 *i*
3	0.0144 *i*

Table III:
Iterations for Larger Initial Impedance

Iteration (k)	Z_{TH} *(p.u.)*
1	0.0170*i*
2	0.0167*i*
3	0.0164*i*
4	0.0160*i*
5	0.0155*i*
6	0.0146*i*

VI. Validating Results in Simulink

Another simulation scenario was implemented with a higher order inverter-based distributed generator (DG) modelled in *MATLAB*/*Simulink*. This model includes the control scheme and parameter values from a real inverter. The control scheme, shown in Fig. 7, regulates real and reactive power by controlling the current of the inverter in the direct and quadrature axis, respectively. By using a PI control, the error between the current set-points and the measured currents was minimized. The inverter-based DG was implemented with the parameter values detailed in Table IV. The inverter-based DG model was connected to the PCC illustrated in Fig. 8.

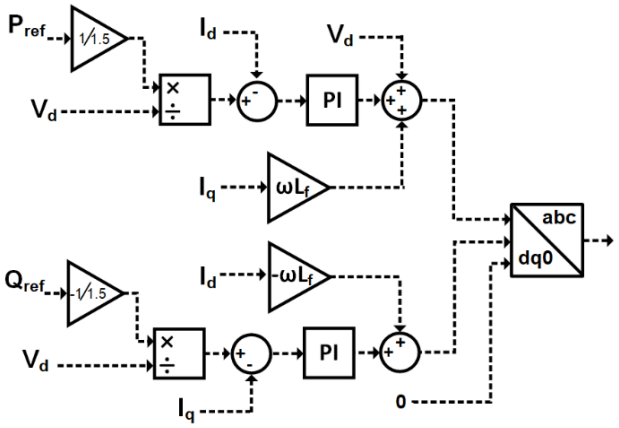

Fig. 7. Block Diagram of the Proposed Current Regulator Control Scheme for Inverter-based DG Implemented in *MATLAB/Simulink*.

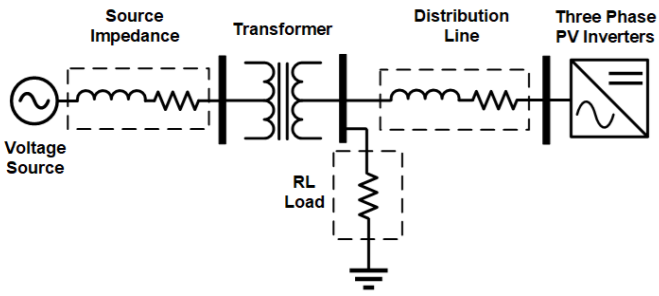

Fig. 8. Point of Common Coupling (PCC) Implemented in MATLAB/Simulink with Equivalent Thevenin Grid Model.

A grid impedance of L_{TH} = 0.182 mH was calculated from the Thevenin equivalent of the grid using a 50 kVA base. The active or real power setpoint from the inverter was changed during the simulation time window. Starting at a 24 kW setpoint and applying a step to 30 kW at 1.2 s. For the first case, the digital twin estimated the grid impedance after 3 iterations starting with a smaller initial impedance value of L_{TH} = 0.159 mH. The iterative process of the digital twin is detailed in Table V. For the second case, a larger initial impedance of L_{TH} = 0.207 mH was selected. The digital twin estimated the equivalent impedance of the grid after 3 iterations. The iteration process is described in Table VI. Fig. 9 through Fig. 12 illustrates the response of the digital twin emulating the measured response of the system using a larger initial impedance. The cost function minimization and impedance parameter estimation for the second case are illustrated in Fig. 13 and Fig. 14, respectively.

TABLE IV:
SIMULATION VALUES FOR INVERTER- BASED DG

Parameter	*Value*	*Units*
R_{DG}	0.1	Ω
L_{DG}	0.7	mH
L_{TH}	0.182	mH
R_L	9.6	Ω
V_{LL}	480	V_{rms}
K_i *(PI)*	563.9	-
K_p *(PI)*	0.1228	-

TABLE V:
ITERATIONS FOR SMALLER INITIAL IMPEDANCE IN SIMULINK

Iteration (k)	L_{TH} *(mH)*	*Cost Function Value*
1	0.159	52.62
2	0.171	23.28
3	0.186	9.78

TABLE VI:
ITERATIONS FOR LARGER INITIAL IMPEDANCE IN SIMULINK

Iteration (k)	L_{TH} *(mH)*	*Cost Function Value*
1	0.207	53.95
2	0.196	32.56
3	0.180	5.80

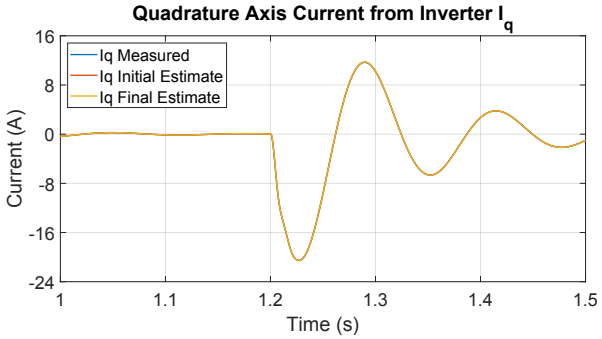

Fig. 9. Quadrature ('Iq') Axis Current from the Inverter Before and After Optimization by the Digital Twin.

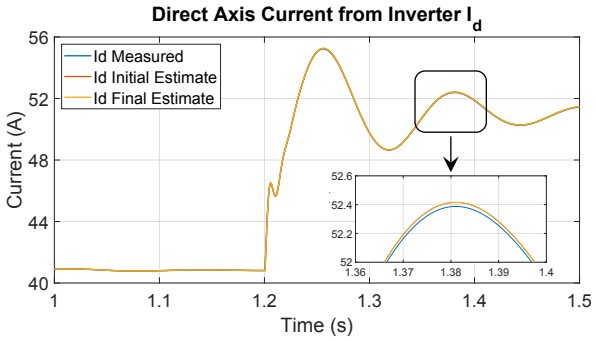

Fig. 10. Direct ('Id') Axis Current from the Inverter Before and After Optimization by the Digital Twin.

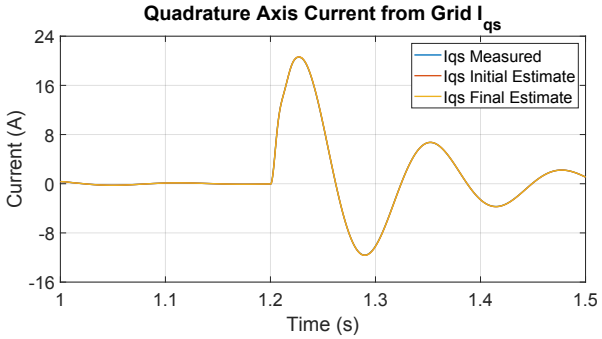

Fig. 11. Quadrature ('Iqs') Axis Current from the Grid Before and after optimization by the Digital Twin.

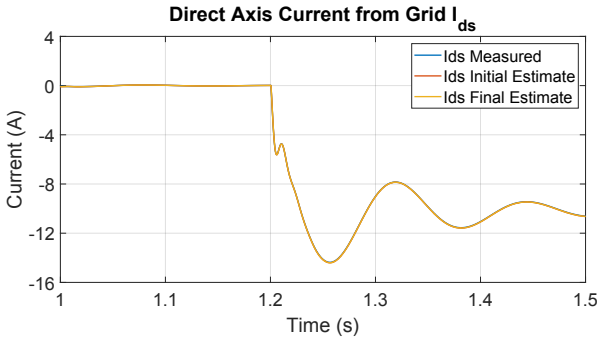

Fig. 12. Direct ('Ids') Axis Current from the Grid Before and After Optimization by the Digital Twin.

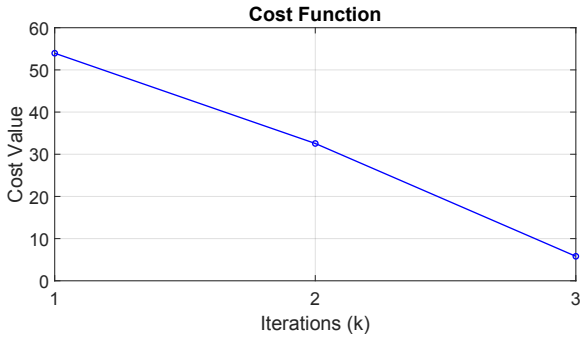

Fig. 13. Cost Function Value Minimization Starting with Larger Initial Impedance.

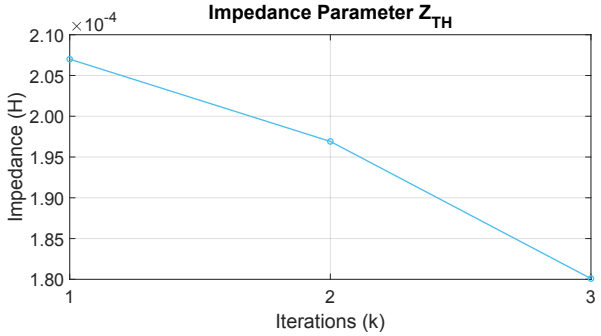

Fig. 14. Impedance Parameter Value Estimation with Larger Initial Impedance of the Digital Twin.

CONCLUSION

The concept of an islanding detection method using a digital twin was proposed and evaluated through simulation scenarios. An optimization method was implemented. The objective of the method was to minimize the difference between the response of the real system and the response from the digital twin. In the process, the estimated equivalent grid impedance value would eventually be useful to help identify both islanded and non-islanded conditions. Simulation results point to minor dependence on the initial impedance selected and a promising first step towards ultimately identify islanding conditions. Further sensitivity analysis is needed i.e., signal noise, delays, errors, etc. Also, it is expected that expanding on the ability of the digital twin to estimate other parameters, such as grid internal *dq0* voltage source representation, will be necessary to support more realistic grid models.

ACKNOWLEDGEMENT

Sandia National Laboratories is a multi-mission laboratory managed and operated by National Technology and Engineering Solutions of Sandia, LLC., a wholly owned subsidiary of Honeywell International, Inc., for the U.S. Department of Energy's National Nuclear Security Administration under contract DE-NA-0003525.

This work was sponsored in part by the Consortium for Hybrid Resilient Energy Systems (CHRES) under grant number DE-NA0003982 from the National Nuclear Security Administration part of the U.S. Department of Energy.

REFERENCES

[1] S. T. Ojetola, *et al.,* "A Real Power Injection Control Strategy for Improving Transient Stability," *2020 IEEE Power & Energy Society General Meeting (PESGM)*, 2020, pp. 1-5.

[2] S. T. Ojetola, J. Wold and D. J. Trudnowski, "A Multi-loop Transient Stability Control via Power Modulation from Energy Storage Device," *IEEE in Transactions on Power Systems* pp. 1-12, 2020.

[3] R. Darbali-Zamora, *et al.*, "Evaluation of Photovoltaic Inverters Under Balanced and Unbalanced Voltage Phase Angle Jump Conditions," *2020 47th IEEE Photovoltaic Specialists Conference (PVSC)*, 2020, pp. 1562-1569.

[4] E. E. Aponte and J. K. Nelson, "Time optimal load shedding for distributed power systems," *IEEE in Transactions on Power Systems*, vol. 21, no. 1, pp. 269-277, Feb. 2006.

[5] O. Arguence, F. Cadoux, B. Raison and L. De Alvaro, "Impact of Power Regulations on Unwanted Islanding Detection," in *IEEE Transactions on Power Electronics*, vol. 33, no. 10, pp. 8972-8981, Oct. 2018.

[6] "IEEE Standard for Interconnection and Interoperability of Distributed Energy Resources with Associated Electric Power Systems Interfaces," IEEE Std 1547-2018, pp. 1–138, 2018.

[7] Y. Yang, P. Enjeti, F. Blaabjerg and H. Wang, "Wide-Scale Adoption of Photovoltaic Energy: Grid Code Modifications Are Explored in the Distribution Grid," in *IEEE Industry Applications Magazine*, vol. 21, no. 5, pp. 21-31, Sept.-Oct. 2015.

[8] A. Pouryekta, V. K. Ramachandaramurthy, N. Mithulananthan and A. Arulampalam, "Islanding Detection and Enhancement of Microgrid Performance," in *IEEE Systems Journal*, vol. 12, no. 4, pp. 3131-3141, Dec. 2018.

[9] A. F. Hoke, A. Nelson, S. Chakraborty, F. Bell and M. McCarty, "An Islanding Detection Test Platform for Multi-Inverter Islands Using Power HIL," in *IEEE Transactions on Industrial Electronics*, vol. 65, no. 10, pp. 7944-7953, Oct. 2018.

[10] P. Du, Z. Ye, E. E. Aponte, J. K. Nelson, and L. Fan, "Positive-Feedback-Based Active Anti-Islanding Schemes for Inverter-Based Distributed Generators: Basic Principle, Design Guideline and Performance Analysis," IEEE in Transactions on Power Electronics, vol. 25, no. 12, pp. 2941-2948, Dec. 2010.

[11] E. Desarden-Carrero, R. Darbali-Zamora, and E. E. Aponte Bezares, "Analysis of Commonly Used Local Anti-Islanding Protection Methods in Photovoltaic Systems in Light of the New IEEE 1547-2018 Standard Requirements," IEEE 46th Photovoltaic Specialists Conference (PVSC), 2019, pp. 2962–2969.

[12] R. Darbali-Zamora, *et al*., "Distribution Feeder Fault Comparison Utilizing a Real-Time Power Hardware-in-the-Loop Approach for Photovoltaic System Applications," *IEEE 46th Photovoltaic Specialists Conference (PVSC)*, 2019, pp. 2916-2922.

[13] R. Darbali-Zamora, *et al*., "State Estimation-Based DER Optimization for Distribution Voltage Regulation in Telemetry-Sparse Environment using a Real-Time Digital Twin", *MDPI Energies*, pp 1-20, Jan 19, 2021.

[14] J. J. Grainger and W. D. Stevenson, Power System Analysis. McGraw- Hill, 1994.

[15] A. J. Wood and B. F. Wollenberg, Power Generation, Operation, and Control. John Wiley & Sons, Inc., 1996.

[16] E. Berrios Galarza, 'Método de Detección de Aislamiento como Apoyo a la Generación Distribuida', Master's Thesis, University of Puerto Rico – Mayagüez, 2013.

[17] J. Duncan Glover, T. Overbye, M. Sarma, Power System Analysis & Design. Cengage Learning, 2017.

[18] P. Krause, O. Wasynczuk, S. Sudhoff, and S. Pekarek, Analysis of Electric Machinery and Drive Systems. John Wiley & Sons, Inc., 2013, pp. 86–120.